Proc. *Computer Vison and Pattern Recognition (CVPR'99)*, Fort Collins, CO, USA,
23-25 June 1999, IEEE Computer Society PR00149, pp. 402–407

Elastic Registration of Medical Images Using Radial Basis Functions with Compact Support

Mike Fornefett, Karl Rohr, and H. Siegfried Stiehl

Universität Hamburg, Fachbereich Informatik,
Arbeitsbereich Kognitive Systeme
Vogt-Kölln-Str. 30, D-22527 Hamburg, Germany
Email: fornefett@informatik.uni-hamburg.de

Abstract

We introduce radial basis functions with compact support for elastic registration of medical images. With these basis functions the influence of a landmark on the registration result is limited to a circle in 2D and, respectively, to a sphere in 3D. Therefore, the registration can be locally constrained which especially allows to deal with rather local changes in medical images due to, e.g., tumor resection. An important property of the used RBFs is that they are positive definite. Thus, the solvability of the resulting system of equations is always guaranteed. We demonstrate our approach for synthetic as well as for 2D and 3D tomographic images.

1. Introduction

Registration is an important technique in medical image analysis. Rigid and affine registration methods can only cope with global differences, for example, translation, rotation, and scaling. In many cases, however, elastic or non-rigid methods are required to cope with local differences between the images. Such differences are due to, for example, scanner-induced deformations, movements of the patient, surgical interventions, or different anatomy (e.g. image atlas-registration).

In this paper, we consider a point-based elastic registration approach based on the radial basis function (RBF) interpolation method. With this approach the transformation is composed of radially symmetric functions that serve as basis functions. The choice of the type of the RBF is crucial for the overall characteristics such as the smoothness or the locality of the transformation function.

Bookstein [2] has introduced thin-plate splines for medical image registration. This approach yields minimal bending energy properties measured over the whole image, but the deformation is not limited to regions where the point landmarks are placed. This behaviour is advantageous for yielding an overall smooth deformation, but it is problematic when rather local deformations limited to image parts are desired. To cope with local deformations, the landmarks have to be well-distributed over the images to prevent deformations in regions where no changes are desired [1].

Others have investigated multiquadrics as RBFs for registration, e.g. [5], and for image deformations [7]. These RBFs have a parameter which controls their locality. However, the function values of multiquadrics are increasing with growing distance from the landmark position and thus the registration result at locations far off the center of the RBF is largely influenced. Other RBFs decrease with growing distance from the landmark position such as inverse multiquadrics, e.g. [7], and the Gaussian, e.g. [1]. Since these RBFs asymptotically approach zero, the global influence is reduced, but it is not spatially limited, i.e. these RBFs have no compact support.

In this paper, we introduce RBFs with compact support for the registration of medical images. The basis functions we employ have a similar shape as the Gaussian, but they have the advantage that their influence is limited around a landmark (in 2D and 3D images on a circle or a sphere, resp.). This property allows the registration of medical images where changes occur only locally. The application scenario we have in mind is the registration of local changes in medical images due to the resection of a tumor or due to other surgical interventions. This approach has also very nice theoretical properties. Actually, for the basis functions we use, it can be shown that the resulting system of equations is always solvable. Thus, we provide an answer to a previously posed question in [1], where Gaussian-shaped RBFs with compact support are sought while solvability is always ensured.

Below, we first give an overview of the general scheme for registration based on RBFs (Sect. 2). In Sect. 3, we introduce an elastic registration scheme using RBFs with compact support and discuss its properties. Finally, in Sect. 4, we present experimental results for 2D and 3D images.

2. Image registration with RBF

In this section, we briefly describe the radial basis function interpolation scheme and discuss its properties depending on the choice of the basis function.

2.1. General scheme

Generally, in registration applications one has to determine a transformation function $\boldsymbol{u} : \mathbb{R}^d \rightarrow \mathbb{R}^d$, where d is the image dimension, e.g. $d = 2, 3$ for 2D and 3D images, resp. An interpolation transformation function $\boldsymbol{u}(\mathbf{x})$ based on point-landmarks must fulfill the following constraints:

$$\boldsymbol{u}(\mathbf{p}_i) = \mathbf{q}_i, \quad i = 1 \dots n, \tag{1}$$

where $\mathbf{p}_i \in \mathbb{R}^d$ constitute a given set of point-landmarks in the source image and $\mathbf{q}_i \in \mathbb{R}^d$ are the corresponding landmarks in the target image. Often, each coordinate of the transformation function is calculated separately, i.e. the interpolation problem $u_k : \mathbb{R}^d \rightarrow \mathbb{R}$ is solved for each coordinate $k = 1 \dots d$ with the corresponding constraints $u_k(\mathbf{p}_i) = \mathbf{q}_{i,k}$. In the following, we write $u(\mathbf{x})$ instead of $u_k(\mathbf{x})$. In 2D, $u(\mathbf{x})$ is calculated separately for $u_1(\mathbf{x})$ and $u_2(\mathbf{x})$ and in 3D for $u_1(\mathbf{x})$, $u_2(\mathbf{x})$, and $u_3(\mathbf{x})$.

If we apply a radial basis function approach, then the interpolation function $u(\mathbf{x})$ generally consists of two parts:

$$u(\mathbf{x}) = \phi_s(\mathbf{x}) + R_s(\mathbf{x}), \tag{2}$$

where $\phi_s(\mathbf{x})$ is a sum of polynomials up to degree p and $R_s(\mathbf{x})$ consists of a sum of RBFs (the index s denotes sum):

$$\phi_s(\mathbf{x}) = \sum_{j=1}^{M} \beta_j \phi_j(\mathbf{x}), \quad R_s(\mathbf{x}) = \sum_{i=1}^{n} \alpha_i R(||\mathbf{x} - \mathbf{p}_i||).$$

Here, the $\phi_j(\mathbf{x})$ are a basis of M functions for all polynomials up to degree p, $R(r) = R(||\mathbf{r}||)$ is a function depending only on the distance $r \geq 0$ from the origin, $||\mathbf{x} - \mathbf{p}_i|| = ||\mathbf{r}||$ is the Euclidean distance from $\mathbf{x}$ to $\mathbf{p}_i$, and α_i and β_j are coefficients. The RBFs $R(||\mathbf{x} - \mathbf{p}_i||)$ are centered around the n landmarks $\mathbf{p}_i$. Inserting (2) in (1) and using the following additional constraints:

$$\sum_{i=1}^{n} \alpha_i \phi_j(\mathbf{p}_i) = 0, \quad j = 1 \dots M,$$

yields the following system of linear equations for the coefficients $\boldsymbol{\alpha} = (\alpha_1, ..., \alpha_n)^T$ and $\boldsymbol{\beta} = (\beta_1, ..., \beta_M)^T$:

$$\begin{pmatrix} \mathbf{K} & \mathbf{P} \\ \mathbf{P}^T & 0 \end{pmatrix} \begin{pmatrix} \boldsymbol{\alpha} \\ \boldsymbol{\beta} \end{pmatrix} = \begin{pmatrix} \mathbf{q}_k \\ 0 \end{pmatrix}, \tag{3}$$

where $\mathbf{K}$ is the $n \times n$ sub-matrix given by $K_{ij} = R(||\mathbf{p}_i - \mathbf{p}_j||)$ and $\mathbf{P}$ the $n \times M$ sub-matrix given by $P_{ij} = \phi_j(\mathbf{p}_i)$. $\mathbf{q}_k = (\mathbf{q}_{k,1}, ..., \mathbf{q}_{k,n})^T$ is a vector of the kth coordinate of the target landmarks $\mathbf{q}_i$.

2.2. Important properties

The choice of the RBF $R(r)$ determines the characteristics of the transformation function $u(\mathbf{x})$. Given the application scenario from above the following properties are of primary interest:

- *Locality.* By locality we denote the spatial range of influence induced by an additionally used landmark pair. These influences can be rather local, i.e. regions of the registration result at larger distances than a certain radius from the landmark pair do not undergo changes. Alternatively, the landmark pair can influence the whole transformed image. Some RBFs have locality parameters which allow to control their influence on the registration result (see also Sect. 2.3 below).
- *Solvability.* To find solutions for the coefficients $\boldsymbol{\alpha}$ and $\boldsymbol{\beta}$ for all possible sets of landmarks, which are not colinear in 2D and not coplanar in 3D, it is required that the matrix on the left hand side of (3) has to be non-singular. We will discuss the non-singularity of the matrix based on the choice of the RBF in Sect. 2.3 below.
- *Efficiency.* Computational efficiency is important especially for large data sets such as 3D images. The computation of a transformation function depends on the used basis function. Also, for efficiently solving the system (3) it is important whether the involved matrix is dense or sparse.

2.3. Commonly used radial basis functions

A variety of different RBFs have been proposed for elastic image registration and image deformation. These are, for example, thin-plate splines (R_{TPS}), e.g. [2, 3, 6], multiquadrics (R_M), e.g. [4, 5, 7], inverse multiquadrics (R_{IM}), e.g. [7], and the Gaussian (R_G), e.g. [1]:

$$R_{TPS}(r) = \begin{cases} r^{4-d} \ln r & 4 - d \in 2\mathbb{N} \\ r^{4-d} & \text{otherwise,} \end{cases} \tag{4}$$

$$R_M(r) = (r^2 + c^2)^{\mu}, \quad \mu \in \mathbb{R}_+, \tag{5}$$

$$R_{IM}(r) = (r^2 + c^2)^{-\mu}, \quad \mu \in \mathbb{R}_+, \tag{6}$$

$$R_G(r) = e^{-r^2/2\sigma^2}. \tag{7}$$

Locality. The first two functions increase, while the latter two functions decrease with growing r from the landmark point. All these functions have in common that they have no compact support and therefore a landmark pair influences the whole registration result.

Solvability. The transformation function (2) has a certain 'polynomial precision', which corresponds to the polynomial part of degree p. Naturally, polynomials have

global influence on the registration result. Therefore, to reduce the global influence it would be advantageous to have no polynomial part. Note, that due to a mathematical property of some of these functions, which is the conditional positive definiteness, certain polynomials are necessary to guarantee the non-singularity of the matrix in (3). For thin-plate splines we have $p = 1 (d = 2, 3)$ and for multiquadrics p depends on the exponent μ. The minimal degree p is $p = \lceil \mu \rceil - 1$ where $\lceil \mu \rceil$ denotes the smallest integer $\geq \mu$. The inverse multiquadric and the Gaussian are positive definite, and thus they can be calculated without any polynomial part.

Efficiency. All functions (4)-(7) involve the calculation of transcendental functions (the logarithm, the exponential, or the square root with $\mu = 0.5$). Also, the matrix (3) is always dense since the functions have no compact support.

3. Image registration using RBF with compact support

The disadvantages of the functions described above are the global influence of a landmark pair on the registration result, the necessary polynomials for some functions, and the necessity of calculating transcendental functions. In this section, we describe a spatially limited RBF which does not have these disadvantages, and is thus suited for our purpose of spatially limited medical image registration.

3.1. ψ-functions of Wendland

We propose to use the $\psi-$functions of Wendland [9] as RBFs for elastic registration of medical images. These radial basis functions have compact support, are positive definite, and are moreover polynomials. These RBFs have previously been used in [8] to model facial expressions for videocoding applications. The general form of the RBFs can be stated as:

$$\psi(r) = \begin{cases} p(r) & 0 \leq r \leq 1 \\ 0 & r > 1, \end{cases} \tag{8}$$

where $p(r)$ is a univariate polynomial. Let $\psi(r)$ denote the univariate function, then $\boldsymbol{\psi} : \mathbb{R}^d \rightarrow \mathbb{R}, \boldsymbol{\psi}(\mathbf{r}) = \psi(||\mathbf{r}||)$ is the corresponding multivariate function in the space of dimension d. The mathematical property of positive definiteness of ψ depends on the space dimension d. If ψ is positive definite on $\mathbb{R}^d$, then ψ is also positive definite on $\mathbb{R}^g$ with $0 < g \leq d$. It has been proven in [9] that for given space dimension d and smoothness $C^{2k}(\mathbb{R})$ there exists – up to a constant factor – only one function $\psi(r)$ of the form (8) which is positive definite on $\mathbb{R}^d$ and which has a polynomial of minimal degree $\lfloor d/2 \rfloor + 3k + 1$, where $\lfloor x \rfloor$, the floor function, is the largest integer $\leq x$. This function is given by:

$$\psi_{d,k}(r) := I^k \, (1 - r)_+^{\lfloor d/2 \rfloor + k + 1}(r) \tag{9}$$

with

$$(1 - r)_+^{\nu} = \begin{cases} (1 - r)^{\nu} & 0 \leq r < 1 \\ 0 & r \geq 1 \end{cases}$$

as the truncated polynomial and

$$I \, \psi(r) := \int_r^{\infty} t \; \psi(t) \, dt \qquad r \geq 0$$

as the integral operator which is applied k times in (9). Note, that for even dimensions d, the property $\psi_{d,k} = \psi_{d+1,k}$ holds due to the floor function in (9). For the functions $\psi_{d,k}(r)$ we chose $d = 3$ which is the largest image dimension in our registration applications. As we have mentioned, the function $\psi_{3,k}$ is positive definite also for smaller dimensions than three. Below, we list ψ-functions for $d = 3$ and $k = 0...2$:

$$\begin{aligned} \psi_{3,0}(r) &= (1 - r)_+^2 \\ \psi_{3,1}(r) &= (1 - r)_+^4 (4r + 1) \\ \psi_{3,2}(r) &= (1 - r)_+^6 (35r^2 + 18r + 3). \end{aligned}$$

In Fig. 1 the functions $\psi_{3,0}$ and $\psi_{3,1}$ are plotted together with the Gaussian.

Since we prefer differentiable and smooth functions at $r = 0$, we exclude $k = 0$ and chose the polynomial $\psi_{3,1}$ for $k = 1$ of next smallest degree for use in registration. The mathematical properties also hold for different spatial supports a:

$$\psi_a(r) = \psi(r/a).$$

3.2. Properties of our registration approach

Locality. In our elastic registration approach we first apply a rigid transformation function computed by a least squares fit to cope with global differences. Second, we apply the $\psi_{3,1}$-function as RBF together with the identity transformation. These RBFs ensure limited locality of each landmark on a circle or a sphere depending on the length a of the support.

Solvability. The $\psi_{3,1}$-functions are positive definite which ensures the regularity of the matrix $\mathbf{K}$. Since an additional polynomial part ϕ_s is not necessary, (3) reduces to:

$$\mathbf{K}\boldsymbol{\alpha} = \mathbf{q}_k \, .$$

Note, that we use an equal support size a for all landmarks. We are not aware of a theoretical result which states that $\mathbf{K}$ in the case of different support sizes a is non-singular. Thus the solvability is not guaranteed.

Efficiency. In comparison to the Gaussian or the inverse multiquadrics neither exponential nor root functions have to be evaluated for the $\psi_{3,1}$-function, which is a polynomial. Also, depending on the size a of the support and the distribution of the landmarks $\mathbf{p}_i$ the matrix $\mathbf{K}$ is rather sparse.

3.3. Comparison with the Gaussian

In Fig. 1, we compare the shape of the ψ-functions $\psi_{a,3,0}(r)$ and $\psi_{a,3,1}(r)$ with the Gaussian. Like all positive definite functions, $\psi(r)$ has its maximum at $r = 0$. For a

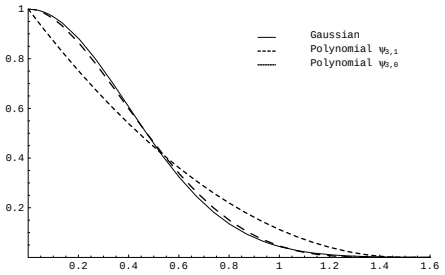

Figure 1: Comparison of $\psi_{a,3,0}, \psi_{a,3,1}$ with $a = 1.504$ with the Gaussian with $\sigma = 0.4$. The similarity is apparent.

given value of σ of the Gaussian we computed a such that the integrals over both functions were equal. This yields:

$$\frac{a}{3} = \sqrt{\pi/2}\,\sigma \qquad \Rightarrow \qquad a = 3\sqrt{\pi/2}\,\sigma.$$

The similarity of the graphs $\psi_{a,3,1}$ and the Gaussian is striking.

3.4. Preservation of topology

A major requirement for an elastic registration scheme is preservation of topology. One necessary condition is that the function $\boldsymbol{u}$ is continuous. Another necessary condition is that the determinant of the Jacobian matrix must be positive at each point of the image:

$$\det(\boldsymbol{u}) > 0.$$

We analyzed the Jacobian matrix for an isolated landmark $\mathbf{p}$ which gives the conditions listed in Tab. 1, where Δ is the displacement from the source landmark $\mathbf{p}$ to the target landmark $\mathbf{q}$ in one coordinate direction. These conditions

Table 1: Minimum a and σ for given displacement Δ.

Dimension	$\psi_{a,3,1}$	$\psi_{a,3,2}$	Gaussian
$d = 2$	$a > 2.98\,\Delta$	$a > 3.54\,\Delta$	$\sigma > 0.86\,\Delta$
$d = 3$	$a > 3.66\,\Delta$	$a > 4.33\,\Delta$	$\sigma > 1.06\,\Delta$

are valid only for isolated landmarks for which no other landmark is placed within the radius a of the support. For landmarks with intersecting support regions the minimal value of a depends also on the positions of the landmarks $\mathbf{p}_i$ which leads to a much more complicated calculation. Nevertheless, Tab. 1 is a good reference and gives a clue for choosing a minimal value for the locality parameter a.

4. Experimental Results

We now present registration results for synthetic and tomographic images using the elastic registration approach introduced in Sect. 3. We first demonstrate the applicability of this approach for simple objects, which shift or scale in elastic material. Second, we show experimental results for a pre-operative image with the corresponding post-operative image after tumor resection.

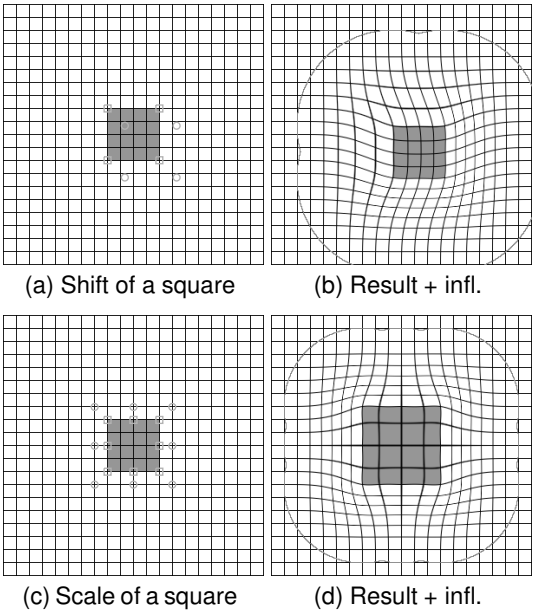

Figure 2: Local elastic registration using $\psi_{3,1}$ as RBF. (a) shift and (c) isotropic scaling of a square. (b) and (d) show registration results together with the area where elastic deformations occur.

In Fig. 2, we demonstrate the registration of objects embedded in elastic material that change their position or form. Landmarks are placed at the outlines, especially at the object corners. These experiments simulate typical medical cases, where image parts shift and either shrink or grow as it happens in cases of, e.g., tumor growth or tumor resection. The grids in Fig. 2 are composed of 301×301 pixels and they are transformed using 4 and 8 landmarks (Figs. 2(a) and (c), resp.). Landmarks of the source and the target image are marked by a box ($\square$) and a circle ($\bigcirc$), resp. Parts of the grids which represent the areas to be registered are colored gray. Source and target landmarks are both shown in the left images. In Fig. 2(a) the landmarks were shifted 20 pixels on both the x- and y-axes to the bottom right. Fig. 2(b) shows the registration result using $\psi_{3,1}$ with a support of $a = 110$ which we found experimentally to be visually the best. We started with the value from Tab. 1 $a = 60$ and proceeded to $a = 180$ using first coarse steps of 30 and then fine steps of 10.

With growing distance outside the square the influences of the landmarks decrease monotonically. The margin where the transformation function reduces to the identity is marked as gray curve. In Fig. 2(c) we demonstrate a scaling example. Fig. 2(d) shows the registration result for $a = 90$ which we found again visually to be the best testing values from 50 to 150. The scaling in the registration result is mainly limited to the square, outside the square again the influences of the landmarks decrease.

Fig. 3 shows an experiment with tomographic images where a tumor in a pre-operative image has to be registered with the corresponding resection area in the post-operative image. An application scenario is the registration of pre-operative tomographic images of high resolution (e.g., MR) with intra-operative images of worse quality (e.g., CT or MR). The aim is to correct the pre-operatively acquired image such that it agree with the current anatomical situation. For demonstration purposes, in our case, we use a post-operative image instead of an intra-operative image. The source image 3(a) and the target image 3(b) are corresponding slices of rigidly transformed 3D MR datasets. In Fig. 3(a), landmarks are placed at the margin of the brain tumor as well as at the outer and inner part of the skin in the vicinity of the tumor. Corresponding target landmarks are shown in Fig. 3(b). The tumor itself corresponds to the resection area. The correspondences between the contours of the skin, the brain, and the tumor have been determined through the use of a snake algorithm. Out of these correspondences we have interactively selected 21 pairs of landmarks shown in Figs. 3(a)-(b). Note, that there is also a significant brain shift at the top of Fig. 3(b) which will not be considered here. For this registration problem a reduction of the influence of the registration scheme far off the area of interest is necessary and thus locality of the registration w.r.t. the tumor is desired. In Fig. 3(c) the transformation result is shown using $\psi_{3,1}$ with $a = 60$ as RBF. Since the maximum displacement in one coordinate direction of the landmark set is 17, the reference value is $a \approx 50$ (Tab. 1). Our experiments revealed that a value of $a = 60$ yielded quite good results, while being close to the reference value and thus ensuring a rather local registration result. To assess the form of the transformation we have applied it to a regular grid which we show in Fig. 3(e). It can be seen that the tumor is registered to the resection area while the region around the tumor is shifted towards the resection area. The reduced influence of the transformation is demonstrated in Figs. 3(d) and (f) where the source image was subtracted from the registration result. To demonstrate the differences to RBFs without compact support we applied the thin-plate spline approach to the same problem as shown in Fig. 3(g). Note, that additional landmarks in other parts of the image are necessary to prevent deformations there. Although we have added 11 of these additional landmarks, thin-plate spline transformations are rather global as it is best seen in the difference image Fig. 3(h). There, the deformations are not limited on the tumor area.

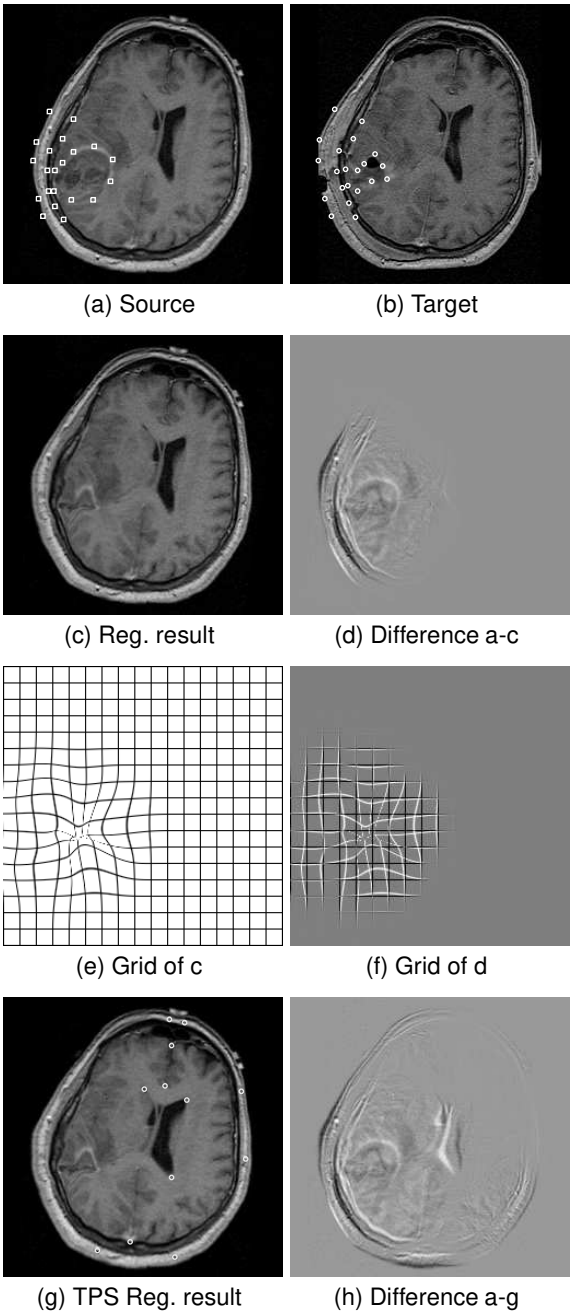

Figure 3: Registration of a tumor with its resection area. (a) Pre-operative image, (b) post-operative image. (c) Registration result and (d) difference between (a) and (c). (e) and (f) same as (c) and (d) for an underlying grid. (g) and (h) Registration result using thin-plate splines with additional landmarks and difference between (a) and (g).

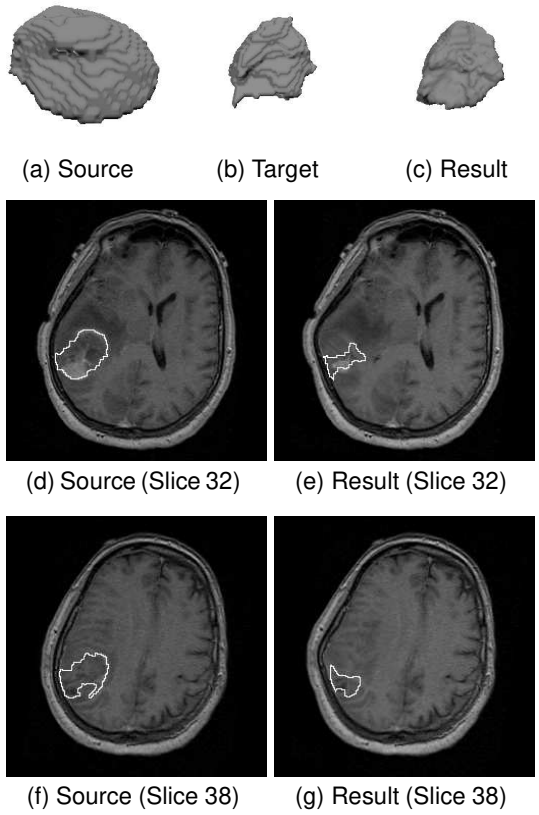

Figure 4: 3D Registration of a tumor with its resection area. (a) and (b) 3D segmentation of the tumor and the resection area as well as (c) 3D registration result showing the transformed tumor only. (d) and (f) show different slices of the 3D source image, (e) and (g) the corresponding slices of the 3D registration result.

In Fig. 4 we demonstrate the applicability of our approach for the case of a 3D registration problem. The outlines of the tumor as well as of the resection area have been determined manually. 40 landmarks have been used and the correspondences have been determined by simply intersecting rays going through the common geometric center point with the corresponding surfaces. First, we segmented the tumor and the resection area as shown in Figs. 4(a) and (b). The registration result is shown in Fig. 4(c) which is quite similar to the target image. Figs. 4(d) and (f) show exemplarily two slices of the 3D dataset together with the outlines of the tumor. The registration result for the same slices is shown in Figs. 4(e) and (g), resp. Also here, the deformation is limited to an area around the tumor.

5. Conclusion

We have proposed an approach to elastic registration which utilizes positive definite functions of compact support as RBF. In comparison to thin-plate spline based elastic registration, with our approach we have a significant reduction of the global influence. The synthetic experiments have shown that object deformations can well be locally registered using landmarks placed at the outlines of the objects. Experiments for 2D and 3D tomographic images have demonstrated the applicability of our approach to registering pre-operative images with post-operative images in the case of tumor resection. Further investigations are necessary to determine appropriate landmark distributions and support sizes of the RBF for registration problems at hand.

Acknowledgements

This work has been supported by Philips Research Hamburg, project IMAGINE (IMage- and Atlas-Guided Interventions in NEurosurgery). The original images in Fig. 3 as well as the tumor outlines have kindly been provided by OA Dr. med. U. Spetzger and Prof.Dr. J.-M. Gilsbach, Dept. of Neurosurgery, Medical School of the University of Technology (RWTH) Aachen.

References

[1] N. Arad and D. Reisfeld. Image warping using few anchor points and radial functions. *Comp. Graphics Forum*, 14(1):35–46, 1995.

[2] F. L. Bookstein. Principal Warps: Thin-Plate Splines and the Decomposition of Deformations. *IEEE Trans. on Pattern Anal. and Machine Intell.*, 11(6):567–585, 1989.

[3] A. C. Evans, W. Dai, L. Collins, P. Neelin, and S. Marrett. Warping of a computerized 3-D atlas to match brain image volumes for quantitative neuroanatomical and functional analysis. *Proc. SPIE 1445*, *Medical Imaging V*, M.H. Loew (Ed.), pp. 236–246, San Jose, CA, 1991.

[4] R. L. Hardy. Multiquadric equations of topography and other irregular surfaces. *J. of Geophys. R.*, 76(8):1905–1915, 1971.

[5] J. A. Little, D. L. G. Hill, and D. J. Hawkes. Deformations Incorporating Rigid Structures. *Computer Vision and Image Understanding*, 66(2):223–232, 1997.

[6] K. Rohr, H. S. Stiehl, R. Sprengel, W. Beil, T. M. Buzug, J. Weese, and M. H. Kuhn. Point-Based Elastic Registration of Medical Image Data Using Approximating Thin-Plate Splines. *Proc. VBC'96, Hamburg, Germany*, K. H. Höhne and R. Kikinis (Eds.), *Lecture Notes in Computer Science 1131*, pp. 297–306, 1996, Springer.

[7] D. Ruprecht and H. Müller. Free form deformation with scattered data interpolation methods. *Comp. Suppl.*, 8:267–281, 1993.

[8] O. Soligon, A. Le Mehaute, and C. Roux. Facial expressions simulation with Radial Basis Functions. *Intern. Workshop on Synthetic – Natural Hybrid Coding and Three Dimensional Imaging, Rhodes, Greece*, pp. 233–236, 5-9 Sep. 1997.

[9] H. Wendland. Piecewise polynomial, positive definite and compactly supported radial functions of minimal degree. *Advances in Computational Mathematics*, 4:389–396, 1995.